Contrib. Astron. Obs. Skalnaté Pleso **56/1**, 87 – 101, (2026)
https://doi.org/10.31577/caosp.2026.56.1.87

Evidence for a stratified accretion disk wind in AGN

P. Marziani[1], E. Bon[2], S. Panda[3], N. Bon[2], A. Del Olmo[4], A. Deconto-Machado[4,5], K. Garnica[6] and D. Dultzin[6]

[1] *INAF, Astronomical Observatory of Padua, Italy (E-mail: Paola.marziani@inaf.it)*

[2] *Belgrade Astronomical Observatory, Serbia*

[3] *International Gemini Observatory, NSF NOIRLab, La Serena, Chile*

[4] *IAA-CSIC, Granada, Spain*

[5] *IASF-INAF, Milan, Italy*

[6] *IA-UNAM, Mexico City, Mexico*

Received: September 24, 2025; Accepted: October 30, 2025

Abstract. We present observational evidence supporting the presence of a stratified accretion disk wind in active galactic nuclei (AGN), based on multi-wavelength spectroscopic analysis of broad and narrow emission lines. The diversity in emission line profiles, ionization potentials, and kinematic signatures suggests a structured outflow emerging from the accretion disk, with different zones contributing to specific spectral features. High-ionization lines (e.g., CIV λ1549) exhibit strong blueshifts and asymmetric profiles indicative of fast, inner winds, while low-ionization lines (e.g., Hβ, MgII λ 2800) show more symmetric profiles consistent with predominant emission from slower, denser regions farther out, although exhibiting systematic blueshifts in quasars radiating at high Eddington ratios. The intermediate ionization lines (e.g., AlIIIλ1860) present a situation that is intermediate in terms of shift amplitudes, although in several super-Eddington candidates radial outflow velocity may reach values comparable to the ones of the high ionization lines. These results are consistent with radiatively driven wind models featuring radial stratification. We made preliminary photoionization modeling assuming unabsorbed radiation emitted from the corona and the hotter disk regions emission or absorbed by a layer of gas. Our findings provide new constraints on the geometry and physical conditions of AGN winds, providing clear evidence in favor of stratified wind emission.

Key words: Supermassive black holes (1663) – Active galactic nuclei (16) – Quasars (1319) – Spectroscopy (1558) – Photoionization (2060)

1. Introduction

The concept of a quasar "main sequence" (MS) emerged from the landmark work of Boroson & Green (1992), who identified a strong anti-correlation between the relative strength of FeIIλ4570 emission and the full width at half

maximum (FWHM) of the broad Hβ line. This relation, commonly expressed through the parameter $R_{\rm FeII}$= FeIIλ4570/Hβ, was first hinted at in earlier works (e.g., Gaskell 1985 and has since been confirmed and extended in a large number of studies (Sulentic et al., 2000a,b; Shen & Ho, 2014; Rakshit et al., 2020; Wu & Shen, 2022). The MS framework provides a powerful tool for organizing the remarkable diversity of type-1 active galactic nuclei (AGN) spectroscopic properties.

Within this scheme, type-1 AGN can be broadly separated into two main populations: Population A and Population B (Sulentic et al., 2000a, 2002, 2011). Population A sources, characterized by narrower Hβ profiles (FWHM $<$ 4000 km s^{-1}), are generally associated with high accretion rates relative to the Eddington limit, while Population B sources (FWHM $>$ 4000 km s^{-1}) are typically lower Eddington ratio ($L/L_{\rm Edd}$, where $L_{\rm Edd}$ is the Eddington luminosity) systems. A small subset, on the order of $\sim$ 10% of the population, represents "extreme" Population A sources ($R_{\rm FeII}>$ 1), which are widely interpreted as candidates for super-Eddington accretion (Wang et al., 2013; Marziani & Sulentic, 2014; Du et al., 2018; Panda & Marziani, 2023; Panda, 2024; Marziani et al., 2025).

The MS is thought to be primarily driven by the Eddington ratio $L/L_{\rm Edd}$ (Marziani et al., 2001; Boroson, 2002; Shen & Ho, 2014; Sun & Shen, 2015; Panda et al., 2019), with orientation effects also playing a significant role in shaping the observed diversity. Black hole mass effects, concomitant with viewing angle effects, become relevant when AGN samples cover a wide range in luminosity (Marziani et al., 2018a; Naddaf et al., 2025). The organization of type-1 AGN properties across the MS has been extensively studied at multiple wavelengths, most prominently within the so-called 4D Eigenvector 1 (4DE1) parameter space introduced by Sulentic et al. (2000c). This framework combines optical, UV, and X-ray measures to capture the multidimensional diversity of quasars, while also providing a physical interpretation in terms of accretion physics and geometry (see Fraix-Burnet et al. 2017 for a summary).

Large surveys, such as the Sloan Digital Sky Survey (SDSS, York et al. 2000), have provided further statistical foundation for these studies. For instance, Zamfir et al. (2010) analyzed $\approx$470 quasars at $z < 0.7$ with average bolometric luminosities $\log L \sim 45.5$ erg/s, confirming the prevalence of the MS trends and strengthening the case for $L/L_{\rm Edd}$ as a primary driver. More recently, refinements in spectral analysis and improved databases have continued to reinforce this picture (e.g., Shen & Ho 2014; Wu & Shen 2022).

In summary, the quasar main sequence organizes type-1 AGN along a continuum of properties primarily governed by Eddington ratio and orientation. At one end of the sequence lie the extreme Population A sources, with the largest FeII strengths and the highest inferred $L/L_{\rm Edd}$ values, plausibly representing systems accreting at or above the Eddington limit. These sources provide critical laboratories for understanding black hole growth under extreme conditions and the broader role of AGN feedback in galaxy evolution (Marziani et al.,

2025). Luminosity and black hole mass ($M_{\rm BH}$) effects appear in sample covering large ranges in luminosity and mass. They can be reconduced to two effects: an increase in the amplitude of shifts with respect to the rest frame observed mainly in high-ionization lines (e.g., Marziani et al., 2016), and a prominent redward asymmetries associated with very massive black holes (Marziani et al., 2009; Marziani, 2023).

In this paper, we first present a brief summary of three recent works dealing with the observations of outflows as diagnosed from the shifts with respect to the rest frame, namely the prototypical CIVλ1549 high-ionization line, the intermediate ionization emission AlIIIλ1860, and the low ionization line of MgIIλ2800 (Sections 2, 3). The three lines are all unresolved doublets associated with the resonance transition $^2P_{\frac{1}{2},\frac{3}{2}} \rightarrow ^2 S_{\frac{1}{2}}$, with parent ionic species of different ionization potential, from $\approx$ 50 eV (CIV) to $\approx$ 25 eV (AlIII) and $\approx$ 15 eV (MgII). We afterwards attempt to explain the observational results by photoionization models focused on the sectors of the MS where the larger amplitude blueshifts are found, namely Population A and extreme Population A (Section 4).

2. CIVλ1549 Shifts and outflows along the quasar main sequence

Systematic blueshifts of the high-ionization CIVλ1549 emission line provide one of the clearest observational signatures of quasar outflows. Early evidence for such features in composite spectra of radio-quiet quasars was strengthened by HST/FOS studies (Marziani et al., 1996; Corbin & Boroson, 1996; Sulentic et al., 2007; Marziani et al., 2010; Leighly & Moore, 2004; Richards et al., 2011; Sulentic et al., 2007; Marziani et al., 2010; Sulentic et al., 2017). These analyses showed that CIV profiles can be decomposed into at least two components: a virialized, symmetric, and generally unshifted component (well represented by a Lorentzian in Population A sources), and a blue-shifted component that is naturally interpreted as emission from an outflowing wind. The latter is best modeled with a skewed Gaussian profile and becomes increasingly prominent at high $R_{\rm FeII}$ values, i.e., in extreme Population A quasars.

Population trends are striking at low z: large blueshifts of $v_{\rm r} < -1000$ km s^{-1} are observed almost exclusively in Population A sources, particularly those with FWHM(Hβ) < 4000 km s^{-1} and strong FeII emission ($R_{\rm FeII} > 1$; Zamfir et al. 2010; Marziani et al. 2010; Richards et al. 2011). In contrast, Population B quasars rarely show strong CIV blueshifts (if we exclude very high luminosity sources), reinforcing the link between high $L/L_{\rm Edd}$ and the presence of radiatively driven winds.

At higher luminosities, large blueshifts persist. Near-infrared spectroscopy of 52 Hamburg–ESO quasars with $1 \lesssim z \lesssim 3$ and $\log L > 47$ erg/s (HE main sequence, HEMS sample) confirmed that strong CIV blueshifts are associated with high Eddington ratios rather than simply high black hole masses or luminosities

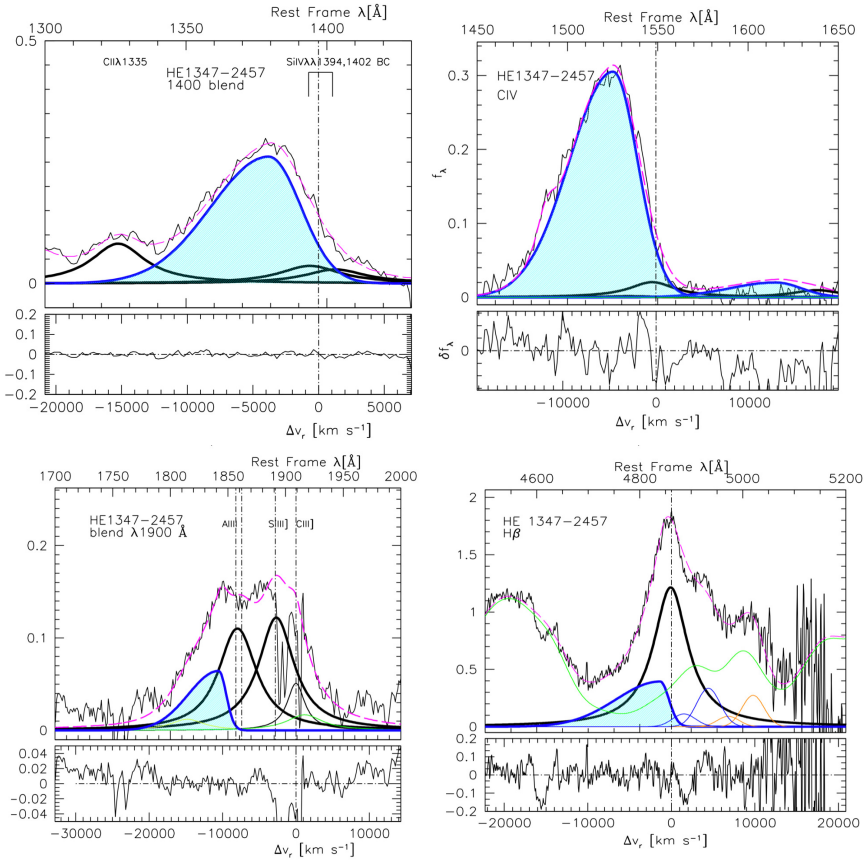

Figure 1. The continuum subtracted spectrum of the luminous Hamburg ESO Main Sequence (HEMS) quasar HE1347-2457, with an emphasis on the outflowing components of SiIVλ1397+OIV]λ1402, CIVλ1549, AlIIIλ1860, Hβ (cyan-shaded components).

(Marziani et al., 2018b; Richards et al., 2011; Giustini & Proga, 2019; Deconto-Machado et al., 2023, 2024). When viewed in the $L/L_{\rm Edd}$–L and $L/L_{\rm Edd}$–$M_{\rm BH}$ planes, blueshift amplitude is most clearly organized by accretion state, with Population A objects (above $L/L_{\rm Edd} \approx 0.2$) being wind-dominated (Marziani et al., 2016).

There is, however, a trend between outflow velocity and luminosity (Marziani et al., 2016; Sulentic et al., 2017). The scaling of outflow velocity with luminosity further supports a radiative-driving mechanism. Weak but consistent correlations ($v \propto L^{0.25}$) are in line with predictions from radiation-driven disk-wind models (Murray et al., 1995; Laor & Brandt, 2002; Proga, 2007b,a). Pop. B at high luminosity also show large blueshifts, up to a few thousands km s^{-1}(Sulentic

et al., 2017). There is evidence of Pop. B outflows at luminosity lower than $\log L \sim 47$ erg/s (e.g., Richards et al. 2011; Marziani et al. 2022a). Since Pop. B shifts at low luminosity remain of small amplitude and difficult to measure, the considerations presented in this paper are meant for Pop. A and extreme Pop. A only.

An example of powerful wind-dominated quasar of the HEMS survey is shown in Fig. 1: the profiles of high ionization lines such as CIVand SiIVλ1397+ OIV]λ1402 are dominated by blueshifted emission associated with the outflows. In this rather extreme cases, the outflows also significantly affect Hβ and the AlIIIλ1860 lines. While the bolometric luminosity sets the available radiative power, it is the Eddington ratio that regulates the efficiency of wind launching and explains the prevalence of large blueshifts in high-$L/L_{\rm Edd}$ sources.

Taken together, the restrictions of large CIV blueshifts to Population A and extreme Population A sources reinforces the interpretation of the quasar main sequence as primarily driven by $L/L_{\rm Edd}$, with CIV outflows providing a direct tracer of radiative wind activity in the broad-line region.

3. Intermediate- and low-ionization lines: AlIIIλ1860 and MgIIλ2800

While the most dramatic blueshifts are observed in high-ionization lines such as CIV, intermediate- and low-ionization species also show systematic kinematic signatures that can provide complementary insights into quasar outflows.

3.1. AlIIIλ1860

The AlIIIλ1860 doublet, with intermediate ionization potential, generally shows only modest outflow signatures compared to CIV. Statistical analyses reveal that AlIIIλ1860 blueshifts are correlated with those of CIV but with a much shallower slope ($\approx$0.1), indicating a less prominent wind contribution (Marziani et al., 2022b; Buendia-Rios et al., 2023). Quantitatively, the median centroid shift of AlIIIλ1860 follows the relation $c(\frac{1}{2})$(AlIII) $\approx$ (0.11 $\pm$ 0.03) $c(\frac{1}{2})$(CIV) + (50 $\pm$ 70) km s^{-1} (Marziani et al., 2022b), consistent with a weaker kinematic response of the intermediate-ionization gas. However, in the most extreme Population A quasars ($R_{\rm FeII} \gtrsim 1$), AlIII can display large blueshifts and asymmetric profiles comparable in strength to those of CIV, suggesting that under super-Eddington conditions the wind dominates across a broader ionization range.

3.2. MgIIλ2800

The MgIIλ2800 resonance doublet, one of the most widely used virial estimators of black hole mass (Marziani et al., 2013a), is typically far less affected by outflows (Trakhtenbrot & Netzer, 2012). Most quasars show symmetric and only weakly shifted MgII profiles. Nonetheless, careful spectral analysis has revealed

subtle displacements of the line core, along with FWHM increases of a few hundred $\mathrm{km\,s^{-1}}$, in the highest L/L_{Edd} extreme Pop. A sources (Marziani et al., 2013b). These modest but systematic shifts indicate that even low-ionization gas can participate in winds under conditions of extreme accretion.

Following Popović et al. (2019), MgIIλ2800 shows Lorentzian MgII profiles and also signatures of outflow, but these are present only in part of the line and not in every source, as already noted by Marziani et al. (2013a). Popović et al. (2019) argue that MgII consists of two kinematic pieces": (i) a core that behaves similarly to Hβ and appears virialized, and (ii) an additional "fountain-like" component, with motions roughly perpendicular to the disc, which produces the very broad wings and can reach shifts of a few thousand $\mathrm{km\,s^{-1}}$. This second component may be associated with a photoionized "bowl" connecting the outer accretion disc and the inner torus (Goad et al., 2012), a configuration that is also consistent with a failed, radiatively accelerated, dusty wind (Czerny & Hryniewicz, 2011; Czerny et al., 2017; Naddaf et al., 2025). Since the fountain component does not correlate with the virial broadening estimators, it is interpreted as due to outflows/inflows rather than rotation.

This configuration can explain the Lorentzian wings of MgIIλ2800. It is, however, not intended to account for the net blueshift of the MgII line core reported by Marziani et al. (2013b) for the highest L/L_{Edd} sources. Those blueshifts are more naturally explained by a systematic line displacement, analogous to what is observed in CIVλ1549, although with a smaller amplitude.

3.3. Ionization potential and the hierarchy of shifts

In extreme Pop. A quasars, v(AlIII) $\approx 0.3\ v$(CIV) (and in some cases they are almost equal), while v(MgII) $\approx 0.1\ v$(CIV) (Marziani et al., 2013b; Buendia-Rios et al., 2025). The comparative behavior of CIVλ1549, AlIIIλ1860, and MgIIλ2800 therefore points to a simple trend: the higher the ionization potential of the line, the larger the blueshift. High-ionization lines such as CIV (IP $\approx$ 47.9 eV) show the largest shifts, often $> -1000\ \mathrm{km\,s^{-1}}$ in extreme Pop. A sources. Intermediate-ionization AlIII (IP $\approx$ 28.4 eV) usually shows smaller shifts, but in the most extreme Pop. A quasars its outflow signature can approach that of CIV. In contrast, the low-ionization MgII doublet (IP $\approx$ 15 eV) shows only modest shifts, typically $\sim$10% of the CIVλ1549 amplitude (Marziani et al., 2013b, 2022b; Buendia-Rios et al., 2023, 2025). This ionization-stratified sequence matches the expectations of disk–wind models, in which the highest-ionization gas traces the fastest parts of the flow, while lower-ionization lines form deeper in the broad-line region, where motions are more nearly virial.

This stratification follows naturally if the high-ionization gas occupies the more accelerated layers of a radiatively driven disk wind close to the continuum source, whereas lower-ionization species arise farther out in the BLR (Murray et al., 1995; Proga, 2007b). In this picture, extreme Population A quasars lie in the regime where radiation pressure not only controls the dynamics of the

highest-ionization gas but also has a measurable impact on intermediate- and even low-ionization lines.

4. Spectral energy distributions of high accretors and photoionization simulations

The interpretation of outflow signatures in high-accretion quasars requires a realistic description of their spectral energy distributions (SEDs). Recent works have established that quasars with high Eddington ratios ($L/L_{\rm Edd} \gtrsim 1$) and extreme FeII emission ($R_{\rm FeII} \gtrsim 1$) exhibit consistent and distinctive SEDs (Jin et al., 2012; Marziani & Sulentic, 2014; Ferland et al., 2020; Panda & Marziani, 2023; Garnica et al., 2025). We utilized the median SED derived from a sample of ≈150 low-redshift Pop. xA quasars (Garnica et al., 2025) as well as the high $L/L_{\rm Edd}$ SED from Jin et al. (2012), and we assume that the line emitting gas is exposed either to the unobscured continuum or continuum absorbed by a hot, dense layer of gas at $r \approx 200 r_{\rm g}$ (for $\approx 10^8$ M$_\odot$; $\log N_{\rm H} = 10^{23}$ cm^{-2}; $\log n_{\rm H} = 10^{11}$ cm^{-3}). A lower black hole mass 10^7 M$_\odot$ appropriate for NLSy1s would require a different, "harder" SED.

4.1. Radiatively driven outflows

Photoionization simulations highlight the conditions under which radiatively driven winds can be launched. Outflows are possible at relatively low column densities ($N_{\rm c} \approx 10^{21}$ cm^{-2}), where radiative acceleration exceeds gravity. The requirement that the force multiplier $M > 2$ translates into the condition $M\,(L/L_{\rm Edd}) > 1$ (see also Ferland et al., 2009; Netzer & Marziani, 2010). At higher column densities ($N_{\rm c} \approx 10^{24}$ cm^{-2}; Ferland & Persson 1989; Panda et al. 2020; Panda 2021), radiation fails to overcome gravity, and the gas remains bound. These results confirm that outflow efficiency is intimately tied to the accretion state and gas structure in the inner broad-line region.

4.2. Predicted emission luminosities and line ratios

The simulations further predict the radial stratification of outflow emission. CIVλ1549 emission is favored at smaller radii, AlIIIλ1860 at intermediate radii, and MgII at larger distances, reflecting both ionization potential and gas density conditions. The luminosities (L(CIV), L(AlIII), L(MgII)) define a narrow "corridor" of optimal ionization parameter where strong emission can be sustained (Fig. 2). The continuum luminosity at $\lambda = 3000$ Å has been assumed to be $\lambda L_\lambda(3000\text{Å}) \approx 4.2 \cdot 10^{44}$ erg/s. The hatched parts identify areas of the parameter plane where radiation forces are insufficient to drive an outflow; dark blue parts are regions where line emission is exceedingly low. The case shown here refers to a partially-absorbed high $L/L_{\rm Edd}$ Jin et al. (2012) continuum, with the absorber located at $r \approx 200 r_{\rm g}$. Due to the relative proximity of the

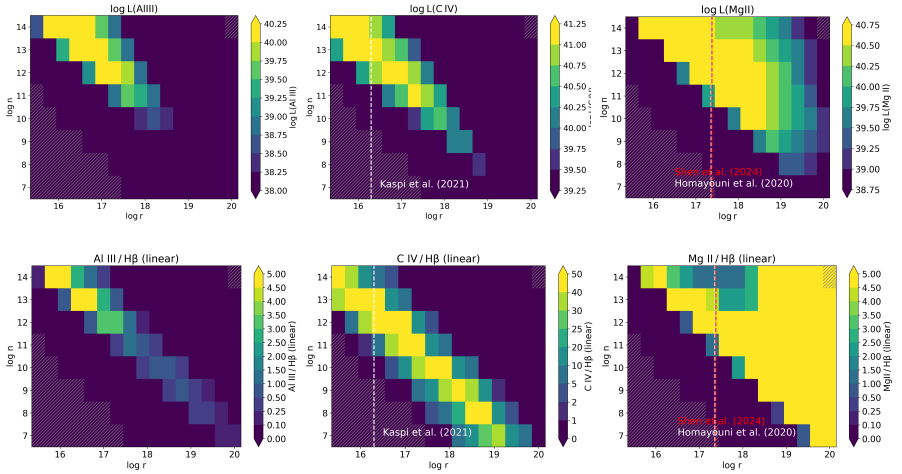

Figure 2. Behavior of line luminosity (top row) and intensity ratios with Hβ (bottom), for CIVλ1549, AlIIIλ1860, and MgIIλ2800 as a function of hydrogen density and radius, for a 10^8 solar masses black hole. The white vertical lines identify the radii measured according to the scaling laws of Kaspi et al. (2021) for CIVλ1549 and Homayouni et al. (2020); Shen et al. (2024) for MgIIλ2800.

absorber relative to the central continuum source, the absorbing gas remains hot and producing significant absorption only in the range between 1 and 10 keV. A fully unabsorbed Jin et al. (2012) continuum would give rise to similar trends.

The corridor peak, if considered at fixed density, is displaced toward larger radii for AlIII, and even more so for MgII with respect to CIV (top row of Fig. 2), as schematically emphasized in Fig. 3. Outside the corridor for CIV and AlIII emission, for radii smaller than the ones of the corridor, over-ionization suppresses line production, a behavior consistent with the observed weakness of CIVλ1549 in extreme Pop. A quasars (Kaspi et al., 2021). For larger radii, under-ionization depresses the emission of both CIVλ1549 and AlIIIλ1860. The behavior of MgIIλ2800 is different: strong emission and large MgIIλ2800/Hβ radii are possible over a wide range of radii that are however larger than the ones where AlIIIλ1860 and CIVλ1549 are maximized.

Predicted line ratios also provide critical tests (bottom panels of Fig. 2). For instance, `CLOUDY` simulations reproduce observed CIVλ1549/Hβ ratios $>$ 10–20

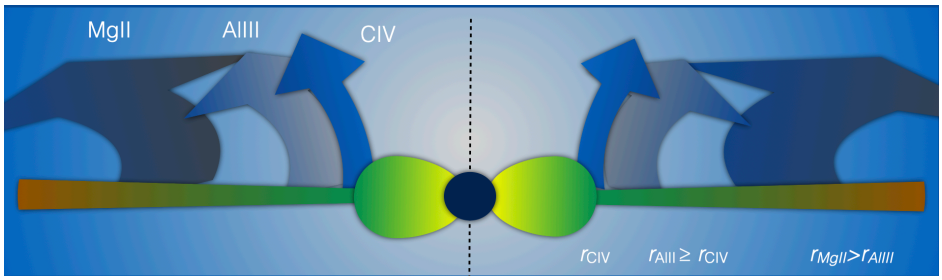

Figure 3. Sketch illustrating the differences in launching radii for the radiatively driven-wind emitting CIVλ1549, AlIIIλ1860, MgIIλ2800. The accretion disk around the central black hole is assumed to have an inner, puffed-up and optically thick region sustained by radiation pressure, as well as an outer thin, optically thick region. The various elements are not drawn to scale.

only under specific combinations of density and ionization, while MgIIλ2800/Hβ ratios match those measured in large quasar samples (Homayouni et al., 2022; Prince et al., 2023). The photoionization model therefore not only explains the ionization-dependent hierarchy of blueshifts (CIVλ1549 > AlIIIλ1860 > MgIIλ2800) but also constrains the physical conditions under which these outflows form.

5. Conclusions

Our analysis of emission-line shifts along the quasar main sequence reinforces the view that radiatively driven outflows are a ubiquitous feature of type-1 AGN. Outflow signatures are present even in single-epoch spectra, and they become dominant in high-ionization lines at high Eddington ratios and, more generally, at the highest luminosities ($L \gtrsim 10^{47}$ erg s^{-1}).

In terms of accretion mode, Pop. A AGN satisfying the criterion $L/L_{\rm Edd} > 0.1 - 0.2$ could be defined as black hole with an inner optically thick, geometrically thick region (c.f., Giustini & Proga, 2019). Among Population A sources, the amplitude of line blueshifts decreases systematically with ionization potential, from CIVλ1549 (C^{3+}) to AlIIIλ1860 and down to MgIIλ2800. While CIVλ1549 blueshifts can exceed several thousand km s^{-1}, MgIIλ2800 shows only subtle but measurable shifts, detectable mainly in extreme Pop. A quasars.

These trends are consistent with an ionization-stratified broad-line region, where higher ionization lines originate closer to the black hole in regions more directly exposed to radiation pressure (Figure 3).

Photoionization simulations with realistic high-accretor SEDs demonstrate that outflows can be launched over a wide range of radii if the column density remains low ($N_c \approx 10^{21}$ cm^{-2}), whereas dense gas ($N_c \approx 10^{24}$ cm^{-2}) remains gravitationally bound. These models reproduce both the hierarchy of shift amplitudes (CIV > AlIII > MgII) and the reverberation-mapped radii of CIVλ1549 and MgIIλ2800 (Homayouni et al., 2020; Khadka et al., 2021; Cao et al., 2022; Shen et al., 2024), providing a physically consistent picture that links SED shape, BLR stratification, and wind dynamics.

Acknowledgements.

S. P. is supported by the international Gemini Observatory, a program of NSF NOIRLab, which is managed by the Association of Universities for Research in Astronomy (AURA) under a cooperative agreement with the U.S. National Science Foundation, on behalf of the Gemini partnership of Argentina, Brazil, Canada, Chile, the Republic of Korea, and the United States of America. A. del Olmo and A. Deconto-Machado acknowledge financial support from the grant PID2022-140871NB-C21 funded by MCIN/AEI/10.13039/501100011033 and by 'ERDF A way of making Europe', and through the Center of Excelence Severo Ochoa grant CEX2021- 515001131-S of the IAA funded by MCIN/AEI/10.13039/501100011033.

References

Boroson, T. A., Black Hole Mass and Eddington Ratio as Drivers for the Observable Properties of Radio-loud and Radio-quiet QSOs. 2002, *ApJ*, **565**, 78, DOI:HEmain10.1086/324486

Boroson, T. A. & Green, R. F., The Emission-Line Properties of Low-Redshift Quasi-stellar Objects. 1992, *ApJS*, **80**, 109, DOI:10.1086/191661

Buendia-Rios, T. M., Marziani, P., Negrete, C. A., & Dultzin, D., Large Binocular Telescope infrared observations of candidate super-Eddington quasars. 2025, *MNRAS*, **540**, 562, DOI:10.1093/mnras/staf694

Buendia-Rios, T. M., Negrete, C. A., Marziani, P., & Dultzin, D., Statistical analysis of Al III and C III] emission lines as virial black hole mass estimators in quasars. 2023, *A&Ap*, **669**, A135, DOI:10.1051/0004-6361/202244177

Cao, S., Zajaček, M., Panda, S., et al., Standardizing reverberation-measured C IV time-lag quasars, and using them with standardized Mg II quasars to constrain cosmological parameters. 2022, *MNRAS*, **516**, 1721, DOI:10.1093/mnras/stac2325

Corbin, M. R. & Boroson, T. A., Combined Ultraviolet and Optical Spectra of 48 Low-Redshift QSOs and the Relation of the Continuum and Emission-Line Properties. 1996, *ApJS*, **107**, 69, DOI:10.1086/192355

Czerny, B. & Hryniewicz, K., The origin of the broad line region in active galactic nuclei. 2011, *A&Ap*, **525**, L8, DOI:10.1051/0004-6361/201016025

Czerny, B., Li, Y.-R., Hryniewicz, K., et al., Failed Radiatively Accelerated Dusty Outflow Model of the Broad Line Region in Active Galactic Nuclei. I. Analytical Solution. 2017, *ApJ*, **846**, 154, DOI:10.3847/1538-4357/aa8810

Deconto-Machado, A., del Olmo, A., & Marziani, P., Exploring the links between quasar winds and radio emission along the main sequence at high redshift. 2024, *A&Ap*, **691**, A15, DOI:10.1051/0004-6361/202449976

Deconto-Machado, A., del Olmo Orozco, A., Marziani, P., Perea, J., & Stirpe, G. M., High-redshift quasars along the main sequence. 2023, *A&Ap*, **669**, A83, DOI:10.1051/0004-6361/202243801

Du, P., Zhang, Z.-X., Wang, K., et al., Supermassive Black Holes with High Accretion Rates in Active Galactic Nuclei. IX. 10 New Observations of Reverberation Mapping and Shortened Hβ Lags. 2018, *ApJ*, **856**, 6, DOI:10.3847/1538-4357/aaae6b

Ferland, G. J., Done, C., Jin, C., Landt, H., & Ward, M. J., State-of-the-art AGN SEDs for photoionization models: BLR predictions confront the observations. 2020, *MNRAS*, **494**, 5917, DOI:10.1093/mnras/staa1207

Ferland, G. J., Hu, C., Wang, J., et al., Implications of Infalling Fe II-Emitting Clouds in Active Galactic Nuclei: Anisotropic Properties. 2009, *ApJL*, **707**, L82, DOI:10.1088/0004-637X/707/1/L82

Ferland, G. J. & Persson, S. E., Implications of CA II emission for physical conditions in the broad-line region of active galactic nuclei. 1989, *ApJ*, **347**, 656, DOI:10.1086/168156

Fraix-Burnet, D., Marziani, P., D'Onofrio, M., & Dultzin, D., The Phylogeny of Quasars and the Ontogeny of Their Central Black Holes. 2017, *Frontiers in Astronomy and Space Sciences*, **4**, 1, DOI:10.3389/fspas.2017.00001

Garnica, K., Dultzin, D., Marziani, P., & Panda, S., The spectral energy distribution of extreme population A quasars. 2025, *MNRAS*, **540**, 3289, DOI:10.1093/mnras/staf862

Gaskell, C. M., Galactic mergers, starburst galaxies, quasar activity and massive binary black holes. 1985, *Nature*, **315**, 386, DOI:10.1038/315386a0

Giustini, M. & Proga, D., A global view of the inner accretion and ejection flow around super massive black holes. Radiation-driven accretion disk winds in a physical context. 2019, *A&Ap*, **630**, A94, DOI:10.1051/0004-6361/201833810

Goad, M. R., Korista, K. T., & Ruff, A. J., The broad emission-line region: the confluence of the outer accretion disc with the inner edge of the dusty torus. 2012, *MNRAS*, **426**, 3086, DOI:10.1111/j.1365-2966.2012.21808.x

Homayouni, Y., Sturm, M. R., Trump, J. R., et al., The Sloan Digital Sky Survey Reverberation Mapping Project: UV-Optical Accretion Disk Measurements with the Hubble Space Telescope. 2022, *ApJ*, **926**, 225, DOI:10.3847/1538-4357/ac478b

Homayouni, Y., Trump, J. R., Grier, C. J., et al., The Sloan Digital Sky Survey Reverberation Mapping Project: Mg II Lag Results from Four Years of Monitoring. 2020, *ApJ*, **901**, 55, DOI:10.3847/1538-4357/ababa9

Jin, C., Ward, M., Done, C., & Gelbord, J., A combined optical and X-ray study of unobscured type 1 active galactic nuclei - I. Optical spectra and spectral energy distribution modelling. 2012, *MNRAS*, **420**, 1825, DOI:10.1111/j.1365-2966.2011.19805.x

Kaspi, S., Brandt, W. N., Maoz, D., et al., Taking a Long Look: A Two-Decade Reverberation Mapping Study of High-Luminosity Quasars. 2021, *arXiv e-prints*, arXiv:2106.00691

Khadka, N., Yu, Z., Zajaček, M., et al., Standardizing reverberation-measured Mg II time-lag quasars, by using the radius-luminosity relation, and constraining cosmological model parameters. 2021, *MNRAS*, **508**, 4722, DOI:10.1093/mnras/stab2807

Laor, A. & Brandt, W. N., The Luminosity Dependence of Ultraviolet Absorption in Active Galactic Nuclei. 2002, *ApJ*, **569**, 641, DOI:10.1086/339476

Leighly, K. M. & Moore, J. R., Hubble Space Telescope STIS Ultraviolet Spectral Evidence of Outflow in Extreme Narrow-Line Seyfert 1 Galaxies. I. Data and Analysis. 2004, *ApJ*, **611**, 107, DOI:10.1086/422088

Marziani, P., Accretion/Ejection Phenomena and Emission-Line Profile (A)symmetries in Type-1 Active Galactic Nuclei. 2023, *Symmetry*, **15**, 1859, DOI:10.3390/sym15101859

Marziani, P., Deconto-Machado, A., & Del Olmo, A., Isolating an Outflow Component in Single-Epoch Spectra of Quasars. 2022a, *Galaxies*, **10**, 54, DOI:10.3390/galaxies10020054

Marziani, P., del Olmo, A., D'Onofrio, M., et al., Narrow-line Seyfert 1s: what is wrong in a name? 2018a, in Proceedings of Science, Vol. **PoS(NLS1-2018)**, *Revisiting narrow-line Seyfert 1 galaxies and their place in the Universe. 9-13 April 2018. Padova Botanical Garden, Italy. Online at ¡A href="https://pos.sissa.it/cgi-bin/reader/conf.cgi?confid=328"¿https://pos.sissa.it/cgi-bin/reader/conf.cgi?confid=328¡/A¿, id.2* (SISSA/ISAS), 002

Marziani, P., Dultzin, D., Sulentic, J. W., et al., A main sequence for quasars. 2018b, *Frontiers in Astronomy and Space Sciences*, **5**, 6, DOI:10.3389/fspas.2018.00006

Marziani, P., Garnica Luna, K., Floris, A., et al., Super-Eddington Accretion in Quasars. 2025, *Universe*, **11**, 69, DOI:10.3390/universe11020069

Marziani, P., Martínez Carballo, M. A., Sulentic, J. W., et al., The most powerful quasar outflows as revealed by the Civ λ1549 resonance line. 2016, *ApSS*, **361**, 29, DOI:10.1007/s10509-015-2611-1

Marziani, P., Olmo, A. d., Negrete, C. A., et al., The Intermediate-ionization Lines as Virial Broadening Estimators for Population A Quasars. 2022b, *ApJS*, **261**, 30, DOI:10.3847/1538-4365/ac6fd6

Marziani, P. & Sulentic, J. W., Highly accreting quasars: sample definition and possible cosmological implications. 2014, *MNRAS*, **442**, 1211, DOI:10.1093/mnras/stu951

Marziani, P., Sulentic, J. W., Dultzin-Hacyan, D., Calvani, M., & Moles, M., Comparative Analysis of the High- and Low-Ionization Lines in the Broad-Line Region of Active Galactic Nuclei. 1996, *ApJS*, **104**, 37, DOI:10.1086/192291

Marziani, P., Sulentic, J. W., Negrete, C. A., et al., Broad-line region physical conditions along the quasar eigenvector 1 sequence. 2010, *MNRAS*, **409**, 1033, DOI: 10.1111/j.1365-2966.2010.17357.x

Marziani, P., Sulentic, J. W., Plauchu-Frayn, I., & del Olmo, A., Is Mg II 2800 a Reliable Virial Broadening Estimator for Quasars? 2013a, *AAp*, **555**, 89, 16pp

Marziani, P., Sulentic, J. W., Plauchu-Frayn, I., & del Olmo, A., Low-Ionization Outflows in High Eddington Ratio Quasars. 2013b, *ApJ*, **764**

Marziani, P., Sulentic, J. W., Stirpe, G. M., Zamfir, S., & Calvani, M., VLT/ISAAC spectra of the Hβ region in intermediate-redshift quasars. III. Hβ broad-line profile analysis and inferences about BLR structure. 2009, *A&Ap*, **495**, 83, DOI:10.1051/0004-6361:200810764

Marziani, P., Sulentic, J. W., Zwitter, T., Dultzin-Hacyan, D., & Calvani, M., Searching for the Physical Drivers of the Eigenvector 1 Correlation Space. 2001, *ApJ*, **558**, 553, DOI:10.1086/322286

Murray, N., Chiang, J., Grossman, S. A., & Voit, G. M., Accretion Disk Winds from Active Galactic Nuclei. 1995, *ApJ*, **451**, 498, DOI:10.1086/176238

Naddaf, M. H., Martínez-Aldama, M. L., Marziani, P., Czerny, B., & Hutsemékers, D., Quasar main sequence unfolded by 2.5D FRADO: Natural expression of Eddington ratio, black hole mass, and inclination. 2025, *A&Ap*, **702**, L13, DOI:10.1051/0004-6361/202556852

Netzer, H. & Marziani, P., The Effect of Radiation Pressure on Emission-line Profiles and Black Hole Mass Determination in Active Galactic Nuclei. 2010, *ApJ*, **724**, 318, DOI:10.1088/0004-637X/724/1/318

Panda, S., The CaFe project: Optical Fe II and near-infrared Ca II triplet emission in active galaxies: simulated EWs and the co-dependence of cloud size and metal content. 2021, *A&Ap*, **650**, A154, DOI:10.1051/0004-6361/202140393

Panda, S., Unveiling the quasar main sequence: illuminating the complexity of active galactic nuclei and their evolution. 2024, *Frontiers in Astronomy and Space Sciences*, **11**, 1479874, DOI:10.3389/fspas.2024.1479874

Panda, S., Małek, K., Śniegowska, M., & Czerny, B., Strong FeII emission in NLS1s: An unsolved mystery. 2020, in IAU Symposium, Vol. **341**, *Panchromatic Modelling with Next Generation Facilities*, ed. M. Boquien, E. Lusso, C. Gruppioni, & P. Tissera, 297–298

Panda, S. & Marziani, P., High Eddington quasars as discovery tools: current state and challenges. 2023, *Frontiers in Astronomy and Space Sciences*, **10**, 1130103, DOI:10.3389/fspas.2023.1130103

Panda, S., Marziani, P., & Czerny, B., The Quasar Main Sequence Explained by the Combination of Eddington Ratio, Metallicity, and Orientation. 2019, *ApJ*, **882**, 79, DOI:10.3847/1538-4357/ab3292

Popović, L. Č., Kovačević-Dojčinović, J., & Marčeta-Mand ić, S., The structure of the Mg II broad line emitting region in Type 1 AGNs. 2019, *MNRAS*, **484**, 3180, DOI:10.1093/mnras/stz157

Prince, R., Zajaček, M., Panda, S., et al., Wavelength-resolved reverberation mapping of intermediate-redshift quasars HE 0413-4031 and HE 0435-4312: Dissecting Mg II, optical Fe II, and UV Fe II emission regions. 2023, *A&Ap*, **678**, A189, DOI:10.1051/0004-6361/202346738

Proga, D., Dynamics of Accretion Flows Irradiated by a Quasar. 2007a, *ApJ*, **661**, 693, DOI:10.1086/515389

Proga, D., Theory of Winds in AGNs. 2007b, in Astronomical Society of the Pacific Conference Series, Vol. **373**, *The Central Engine of Active Galactic Nuclei*, ed. L. C. Ho & J.-W. Wang, 267

Rakshit, S., Stalin, C. S., & Kotilainen, J., Spectral Properties of Quasars from Sloan Digital Sky Survey Data Release 14: The Catalog. 2020, *ApJS*, **249**, 17, DOI:10.3847/1538-4365/ab99c5

Richards, G. T., Kruczek, N. E., Gallagher, S. C., et al., Unification of Luminous Type 1 Quasars through C IV Emission. 2011, *AJ*, **141**, 167, DOI:10.1088/0004-6256/141/5/167

Shen, Y., Grier, C. J., Horne, K., et al., The Sloan Digital Sky Survey Reverberation Mapping Project: Key Results. 2024, *ApJS*, **272**, 26, DOI:10.3847/1538-4365/ad3936

Shen, Y. & Ho, L. C., The diversity of quasars unified by accretion and orientation. 2014, *Nature*, **513**, 210, DOI:10.1038/nature13712

Sulentic, J., Marziani, P., & Zamfir, S., The Case for Two Quasar Populations. 2011, *Baltic Astronomy*, **20**, 427

Sulentic, J. W., Bachev, R., Marziani, P., Negrete, C. A., & Dultzin, D., C IV λ1549 as an Eigenvector 1 Parameter for Active Galactic Nuclei. 2007, *ApJ*, **666**, 757, DOI:10.1086/519916

Sulentic, J. W., del Olmo, A., Marziani, P., et al., What does CIVλ1549 tell us about the physical driver of the Eigenvector quasar sequence? 2017, *A&Ap*, **608**, A122, DOI:10.1051/0004-6361/201630309

Sulentic, J. W., Marziani, P., & Dultzin-Hacyan, D., Phenomenology of Broad Emission Lines in Active Galactic Nuclei. 2000a, *ARA&A*, **38**, 521, DOI:10.1146/annurev.astro.38.1.521

Sulentic, J. W., Marziani, P., Zamanov, R., et al., Average Quasar Spectra in the Context of Eigenvector 1. 2002, *ApJL*, **566**, L71, DOI:10.1086/339594

Sulentic, J. W., Marziani, P., Zwitter, T., Dultzin-Hacyan, D., & Calvani, M., The Demise of the Classical Broad-Line Region in the Luminous Quasar PG 1416-129. 2000b, *ApJL*, **545**, L15, DOI:10.1086/317330

Sulentic, J. W., Zwitter, T., Marziani, P., & Dultzin-Hacyan, D., Eigenvector 1: An Optimal Correlation Space for Active Galactic Nuclei. 2000c, *ApJL*, **536**, L5, DOI:10.1086/312717

Sun, J. & Shen, Y., Dissecting the Quasar Main Sequence: Insight from Host Galaxy Properties. 2015, *ApJL*, **804**, L15, DOI:10.1088/2041-8205/804/1/L15

Trakhtenbrot, B. & Netzer, H., Black hole growth to z = 2 - I. Improved virial methods for measuring M_{BH} and L/L_{Edd}. 2012, *MNRAS*, **427**, 3081, DOI:10.1111/j.1365-2966.2012.22056.x

Wang, J.-M., Du, P., Valls-Gabaud, D., Hu, C., & Netzer, H., Super-Eddington Accreting Massive Black Holes as Long-Lived Cosmological Standards. 2013, *Physical Review Letters*, **110**, 081301, DOI:10.1103/PhysRevLett.110.081301

Wu, Q. & Shen, Y., A Catalog of Quasar Properties from Sloan Digital Sky Survey Data Release 16. 2022, *ApJS*, **263**, 42, DOI:10.3847/1538-4365/ac9ead

York, D. G., Adelman, J., Anderson, John E., J., et al., The Sloan Digital Sky Survey: Technical Summary. 2000, *AJ*, **120**, 1579, DOI:10.1086/301513

Zamfir, S., Sulentic, J. W., Marziani, P., & Dultzin, D., Detailed characterization of Hβ emission line profile in low-z SDSS quasars. 2010, *MNRAS*, **403**, 1759, DOI:10.1111/j.1365-2966.2009.16236.x